

Supplementary Online Material

ScP waveform broadening and attenuation estimates

Observed *ScP* waveforms are typically broadened compared to *P*, with significant variability, most likely due to lower mantle attenuation where the *P* and *ScP* paths most significantly diverge. We document differential attenuation between *P* and *ScP* by finding the best-fit t^* operator (a parameter representing the path integrated attenuation) that maps the direct *P* wave into observed *ScP*, in an event-by-event fashion. Some examples are shown in Supplementary Figure **a-c**. A lower mantle lacking anomalously high attenuation, such as in PREM, yields a differential t^* of ~ 0.15 . Some data in the north of our study area are PREM-like ($t^* < 0.2$), though most *ScP* waveforms require larger t^* values ($0.2 < t^* < 0.6$), and are seen throughout the study area (Supplementary Figure **b**). Some exceptionally large t^* values ($t^* > 0.6$) are required in a region just north of the ULVZ identified in this study. Significantly high attenuation throughout the lowermost few 100 km of the mantle can match these values, though we note that *ScP* can also be broadened by a thin ULVZ (~ 3 km) from an interference phenomena between *ScP* and the wave that reflects off the CMB as a *S* wave, then converts to a *P* wave at the top of the ULVZ (*ScsP*). At present, the thinnest detectable ULVZ with *ScP* precursor analysis is 4 km, and therefore the accumulation of large t^* values north of our *ScP* precursor zone (~ -24.5 deg latitude) might be interpreted as an undetectably thin ULVZ (a northerly thinning of the main ULVZ). Higher frequency data will allow a better vertical resolution in this region. Data to the south, however, do not support such thinning, but we have sparse data coverage there.

Supplementary Figure 1 Caption: Attenuation modeling of broadened *ScP* waveforms. *ScP* and predicted *ScP* from *P*-waveform and t^* -value. **a**, Predicted waveforms for $t^* \leq 0.2$ (PREM-like). **b**, As A for $0.2 < t^* \leq 0.6$. **c**, As a for $t^* > 0.6$. **d**, Map of t^* values for the levels shown in A-C.

Supplementary Figure 2 Caption: Synthetic waveforms for varying ULVZ parameters. The Gaussian Beam method has been utilized, where all important additional reflections and conversions have been included in the waveform synthesis. For the relatively high frequencies present in our array data, this method was computationally advantageous over more complete wavefield approaches, such as the full wave or reflectivity methods, which are cost and time prohibitive to use at 1 Hz dominant energy for the hundreds of models tested here. For the panels that follow, the observed precursor summation trace is shown at the bottom of each panel. Velocity and density changes are given relative to PREM. **a** Synthetics for fixed parameters $\alpha = -10\%$, $\beta = -10\%$ and ULVZ thickness $D = 8.5$ km. Density ρ is varied between -10% and $+20\%$. **b** As (**a**) but for $\alpha = -10\%$ and $\beta = -25\%$. **c** Synthetics for fixed parameters $\alpha = -10\%$, $\rho = +10\%$ and ULVZ thickness $D = 8.5$ km. S-velocity β is varied from 0% to -40% . **d** Synthetics for fixed parameters $\beta = -25\%$, $\rho = 0\%$ and ULVZ thickness $D = 8.5$ km. P-velocity α is varied between 0% and -20% . **e** Same as (**d**) but for $\rho = +10\%$. **f** Synthetics for a fixed $\alpha:\beta$ ratio of 1:1. Density $\rho = +10\%$ and $D = 8.5$ km. Velocities are varied from

–2% to –14%. **g** Same as **(f)** but for $\alpha:\beta = 1:3$. **h** Synthetics for varying thickness (2 km to 18 km) with $\alpha = -10\%$, $\beta = -25\%$ and $\rho = 0\%$. **i** Same as **(h)** but for $\rho = +10\%$. These examples illustrate the robustness of our solution parameters of $(\alpha,\beta,\rho,D)=(-8,-25,+10,8.5)$, while exhibiting some trade off is also present in the modeling (typically less than 2-3 percent for the velocities and density, and less than 1 km for the ULVZ thickness).

Upwelling flow estimates

In the dense layer, radial pressure gradients $\frac{\partial p}{\partial r}$ caused by buoyancy forces will be

balanced by viscous stresses induced by the upwelling flow, $\mu \frac{\partial^2 u_r}{\partial z^2}$, where μ is

viscosity, u_r is velocity in the radial direction, and z indicates the vertical direction. An

estimate of the pressure gradient is $\frac{\Delta \rho g h}{R}$, where h and R are the thickness and radial

extent of the dense layer, respectively. An estimate of the balancing viscous stresses is

$\frac{\mu U}{h^2}$, where U characterizes upwelling velocity. We thus have

$$U \sim \frac{\Delta \rho g h^3}{R \mu}.$$

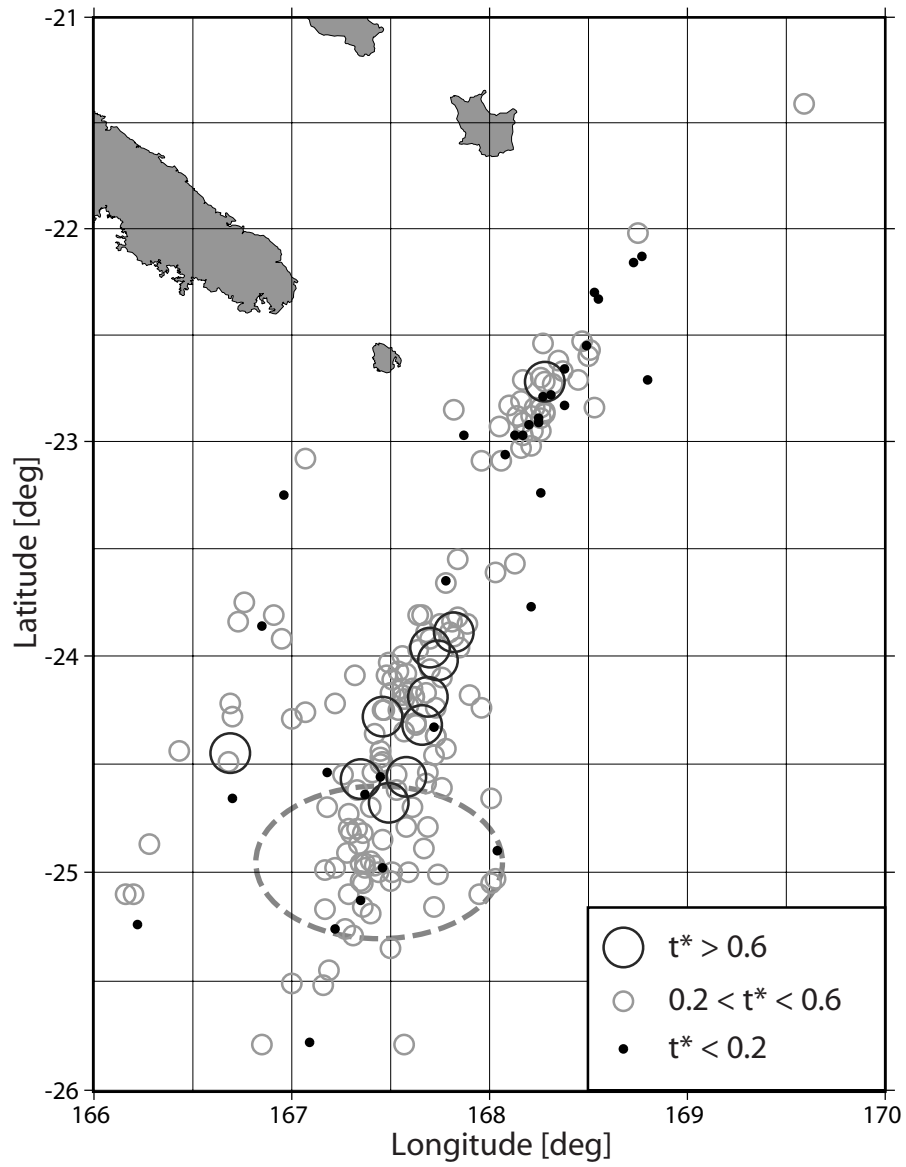
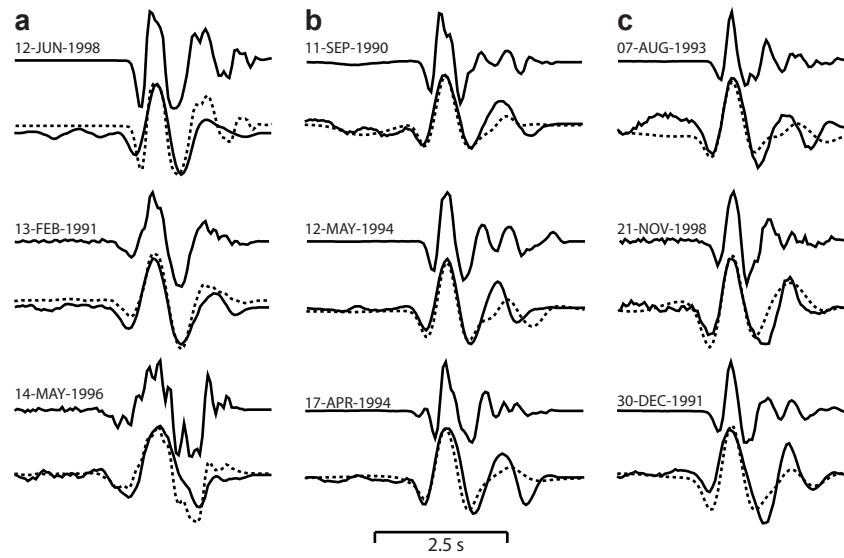
Observations constrain $\Delta \rho$, h and R to be 500 kg/m³, 8 km and 30 km, respectively.

Choosing $\mu = 10^{19}$ Pas implies plausible velocities of $O(10^{-1})$ m/yr.

Supplementary Table 1

Earthquake locations for events, that show the coherent *ScP* precursory energy 1.8 sec before *ScP*, displayed as blue traces in Figure 1C.

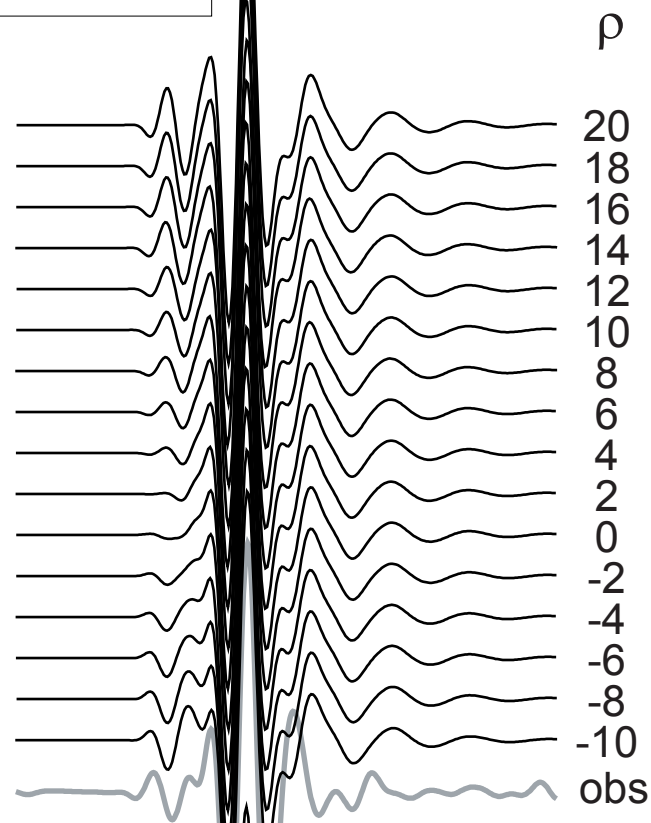
<i>Origin Time</i>	<i>Latitude [deg]</i>	<i>Longitude [deg]</i>	<i>Depth [km]</i>	<i>m_b</i>
02-FEB-1991_21:15:51.020	-24.520	179.740	518.1	4.6
02-JUN-1991_16:25:27.750	-24.957	-179.974	509.8	5.1
02-SEP-1991_15:32:57.610	-25.210	179.910	495.9	4.7
05-OCT-1995_09:23:09.580	-25.072	179.987	501.2	4.6
06-SEP-1993_13:28:57.220	-25.211	-179.967	487.3	4.9
07-JAN-1993_18:35:03.680	-24.994	-179.940	506.8	4.9
10-DEC-1995_21:29:10.950	-24.520	179.790	546.8	4.5
11-DEC-1994_09:29:02.780	-24.793	-179.002	390.8	5.5
11-JUN-1996_14:29:13.470	-24.825	179.938	503.0	4.5
11-OCT-1993_07:55:59.070	-25.041	-179.906	526.6	4.9
11-SEP-1990_13:56:48.360	-24.990	-179.980	558.0	4.8
12-JUN-1998_20:51:02.310	-24.795	179.923	499.8	5.2
12-SEP-1992_19:40:52.560	-25.214	179.815	497.7	4.7
16-AUG-1994_07:16:52.850	-24.660	179.790	532.5	4.7
17-NOV-1996_17:35:53.650	-24.992	179.670	565.9	4.6
21-DEC-1995_07:06:22.500	-24.540	179.848	544.0	4.6
22-DEC-1998_22:07:53.960	-25.160	179.630	518.0	5.6
22-JAN-1998_20:53:34.390	-24.980	-179.750	502.7	4.6
27-NOV-1993_22:25:16.330	-25.248	-179.968	511.8	5.1
29-JUL-1992_08:20:33.380	-24.952	179.933	516.2	4.9
29-MAR-1993_08:25:45.970	-24.946	179.984	506.5	5.1
30-JUN-1997_23:00:12.350	-24.750	179.860	509.8	4.7
31-MAR-1995_15:50:08.290	-25.220	-179.850	481.3	4.9



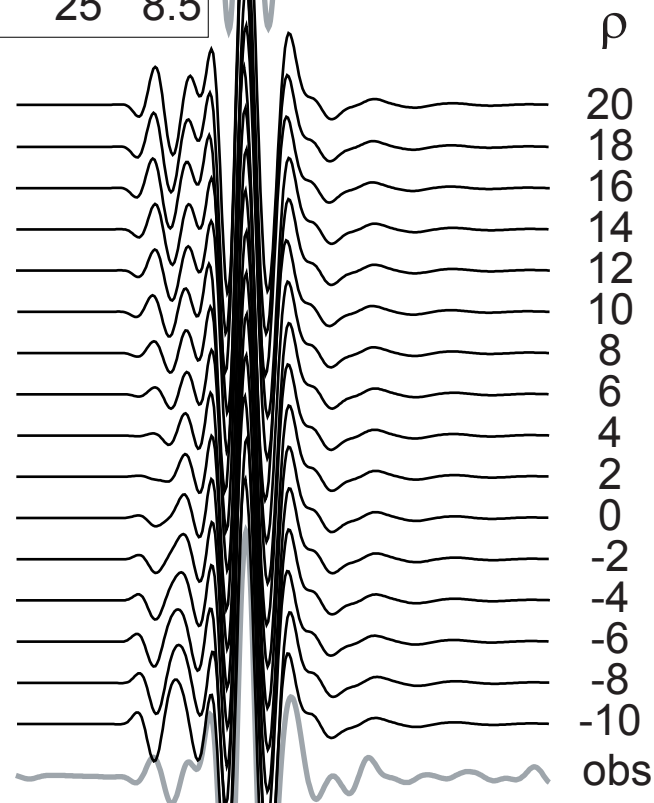
Supplemental Figure 1 [Rost et al., 2005]

a

α	β	D
10	10	8.5

**b**

α	β	D
10	25	8.5

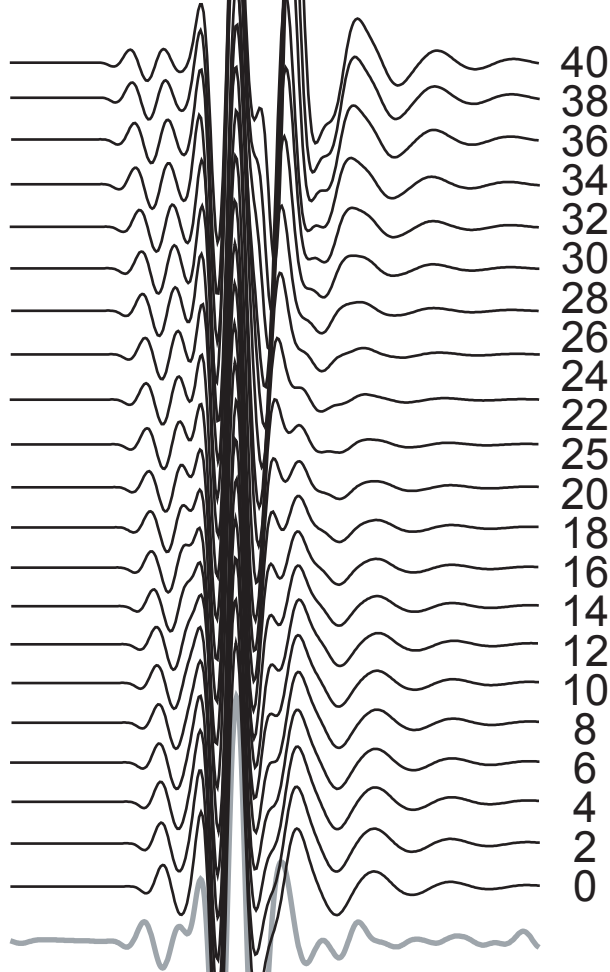


5 s

c

α	ρ	D
10	10	8.5

β

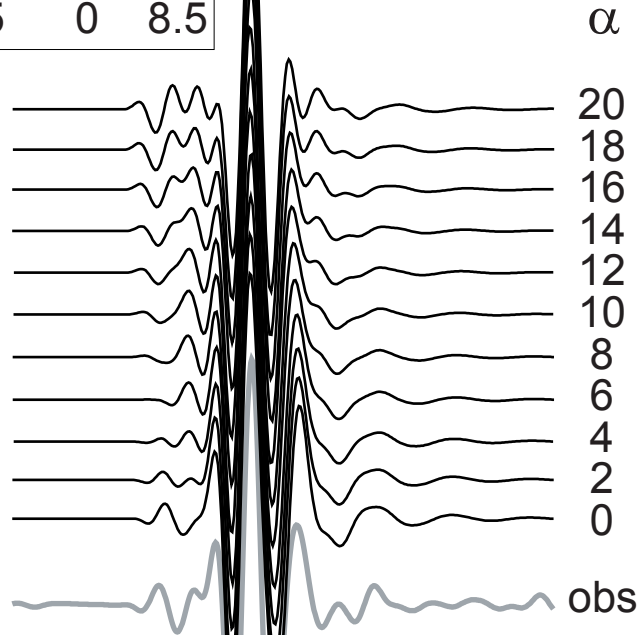


5 s

Supplementary Figure 2c
Rost et al. [2005]

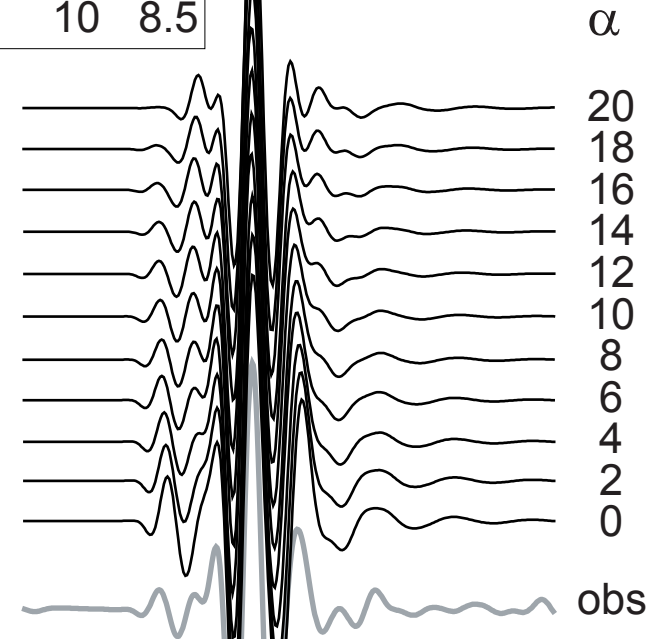
d

β	ρ	D
25	0	8.5



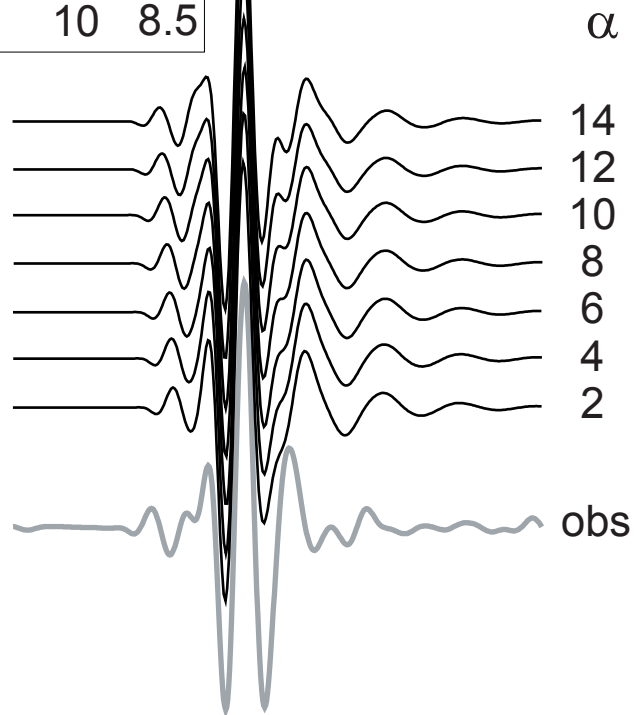
e

β	ρ	D
25	10	8.5



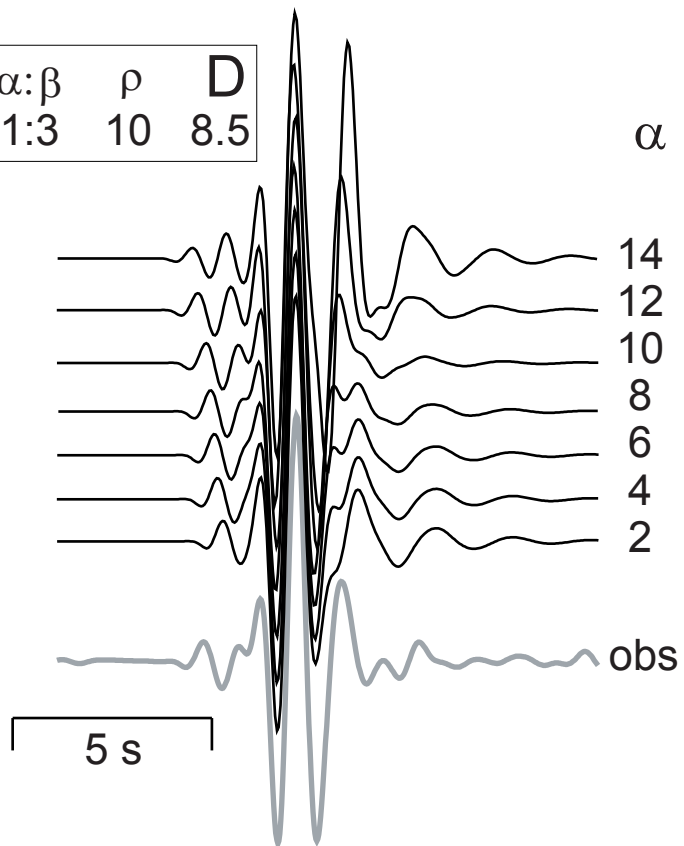
f

$\alpha:\beta$	ρ	D
1:1	10	8.5



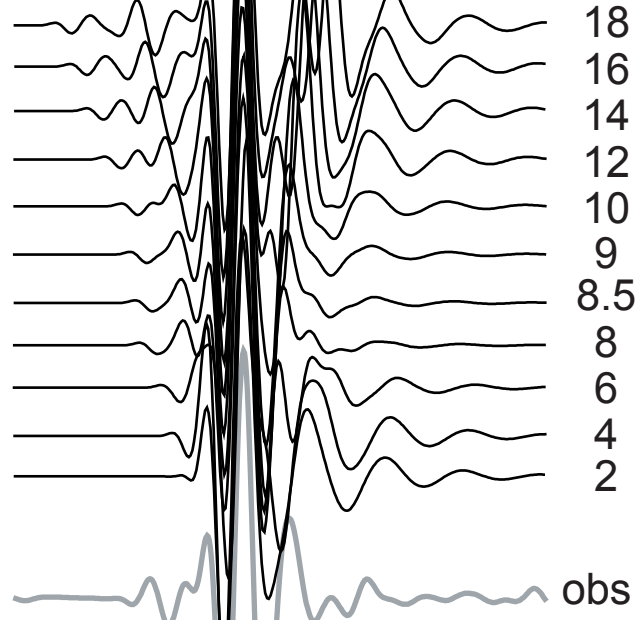
g

$\alpha:\beta$	ρ	D
1:3	10	8.5

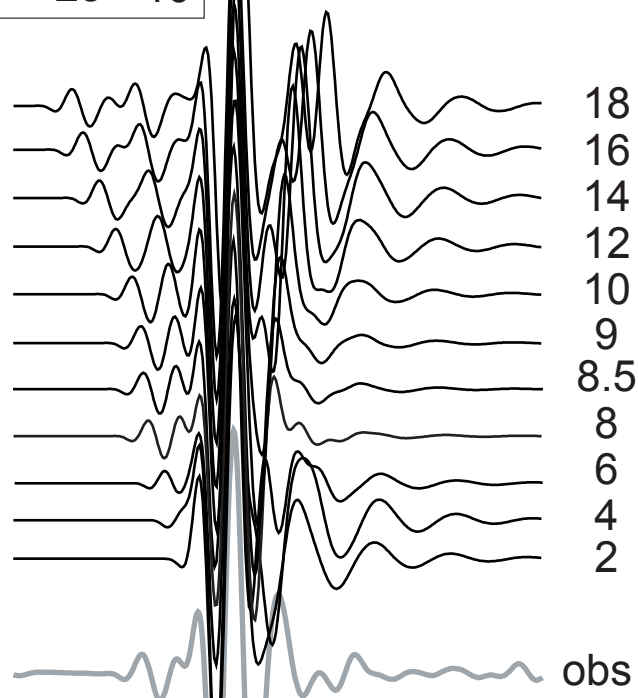


h

α	β	ρ
10	25	0

D**i**

α	β	ρ
10	25	10

D

5 s